M R S Internet Journal of Nitride Semiconductor Research

Volume 2, Article 3

Temperature-Composition Dependence of the Bandgap and Possible Non-complanar Structures in GaN-AlN, GaN-InN and InN-AlN Mixed Crystals

E. V. Kalashnikov
Institute of Mechanical Engineering, RAN

V. I. Nikolaev
Ioffe Physical-Technical Institute

This article was received on May 31, 1996 and accepted on January 24, 1997.

Abstract

The virtual crystal approximation has been used to determine the temperature-composition dependence of the GaN-AlN, GaN-InN, and InN-AlN band gap energies. Also, the thermodynamic instability states in the mixed crystals were studied. The expression for the band gap of mixed A-B crystals has been derived: $E_g^{AB} = (1-x)E_g^A + xE_g^B - bS_{xx}$, where E_g^A and E_g^B are the direct gaps for compounds A and B, respectively, and x is the alloy concentration. The term $S_{xx} \sim T_0/(\partial^2 G/\partial x^2)$ where G is the thermodynamic potential of the mixed crystal, b is a bowing parameter, and T_0 has the meaning of a growth temperature.

1. Introduction

Recent progress in the nitride semiconductors is connected with the realization of high-quality AlGaN and InGaN crystal layers and their application to high brightness light-emitting diodes (LEDs) operating from the near ultraviolet (~3.4 eV) to yellow (~2.1 eV) [1] [2]. The bright emission of the LEDs is associated with direct band-to-band transitions in unstrained InGaN quantum wells [2] in which the InN mole fraction is varied from 0 - 70%.

It is obvious that the band gap (E_g) of semiconductor alloys (mixed crystals) is strongly composition dependent. However, theoretically the alloy bandgap can only be solved at small deviations from the pure components. Experimental E_g values have been measured in nitride alloys throughout the entire compositional range [1] [2] [3] [4] [5] [6] [7] by optical absorption spectroscopy and edge luminescence measurements. The compositional dependence of the band gap is generally described by a parabolic function of the molar fraction x:

$$E_g = xE_{gA} + (1-x)E_{gB} - b \cdot x(1-x) \qquad (1)$$

where E_g^A and E_g^B are the band gaps of the pure components, and b is the bowing parameter. To be more precise we have to note that the term containing x(1-x) is reasonable based on the assumption that the mixed crystal is an ideal solid solution. This approximation is well suited to mixed crystals at small concentrations of one component or at very high temperature where the interactions between the A and B components can be neglected. Larger concentrations of both components usually lead to additional ordering, and in some respects these alloys can be likened to the order in a liquid where Brillouin zones have no conventional meaning. Derivation of the compositional dependence of E_g under these conditions requires special theoretical analysis and calculations.

2. Correction of the Compositional Dependence of the Band Gap

Experiments [8] show that the group III nitride alloys are substituted solid solutions in the cation sublattice of $A_{1-x}B_x$

https://doi.org/10.1557/S1092578300001290 Published online by Cambridge University Press

Experiments [8] show that the group III nitride alloys are substitutional solid solutions in the cation sublattice of $A_{1-x}B_xN$. That is why the $A_{1-x}B_xN$ complexes can be thought of in the following as binary $A_{1-x}B_x$ solutions. To derive the expression for $E_g(x)$ for the solution we apply the virtual-crystal approximation [9]. By considering all possible electron scattering in the conduction band, averaging over random distributions of interacting A and B atoms, and expressing the compositional fluctuations through the thermodynamic potential (G), we can derive the general relation:

$$E_g = (1-x)\cdot E_{gA} + x\cdot E_{gB} - b\cdot S_{xx} \tag{2}$$

$$S_{xx} = < \Delta x(r')\cdot \Delta x(r) > = \frac{NKT}{(\partial^2 G / \partial x^2)_{p,T}}$$

in which [10] where r is a space coordinate, K, N, T, P are the Boltzmann constant, the number of atoms per mole, the temperature and the pressure, respectively. The brackets (< >) denote the averaging over all lattice sites.

In particular G is expressed as $G = (1-x)\cdot G_A + x\cdot G_B + KT[x\cdot \ln x + (1-x)\cdot \ln(1-x)]$ if A-B alloy is an ideal solution. In this case (2) reverts to the traditional formula (1), where $< \Delta x(r')\cdot \Delta x(r) > \equiv x\cdot(1-x)$.

To discuss the main features of (2), mixed crystals are considered for simplicity within the framework of the Williams-Bragg (or regular solution) approximation. This simply means that we neglect the compositional dependence of the compressibility, and G is assumed to be roughly equal to the free energy (F). The thermodynamic potential written for regular solutions has an added term equal to x(1-x)W. The value of W can be expressed as an interaction energy between pairs of different atoms. These energies were calculated in terms of the electronegativities (c) and solubility parameters (d) of the pure elements,

$$\Omega_{\alpha\beta} = \frac{V_\alpha V_\beta}{(N_\alpha V_\alpha + N_\beta V_\beta)}\left[(\delta_\alpha - \delta_\beta)^2 - \frac{3\cdot 10^4 (\chi_\alpha - \chi_\beta)^2}{(V_\alpha V_\beta)^{\frac{1}{2}}}\right] \tag{3}$$

where V_a and V_b are the molar volumes.

Although this equation was used earlier for the calculation of the energy in liquid solutions [11], we are sure that the parameters c, d, and V are weakly dependent on any phase state of the solutions. Moreover it would be expected that the atomic structure of the nitrides has no serious distortions during cooling from the growth temperature. These reasonable assumptions allow us to link S_{xx} with the actual crystal growth temperature.

The analysis of the behavior of G (or F) and S_{xx} at various temperatures indicates the possibility of alloy decomposition at some mole fraction. Figure 1 schematically demonstrates the thermodynamic diagram for a regular solution. The diagram region where the solution is unstable (labile) is captured by the spinodal (curve 2). Alloys grown at temperatures and compositions in the range under the spinodal are spatially inhomogeneous. An example of the compositional dependence F(x) for these alloys is also shown in figure 1. The critical temperatures for $A_{III}B_V$ alloys were calculated using $T_c = W/2R$ [11]. The nitride T_c values are shown in table 1. The compositional dependences of S_{xx} at various temperatures are shown in figure 2. It should be noted that $S_{xx}(x)$ is a pointwise discontinuous function in the area captured by the spinodal (curve 2 in figure 1). The points "a" and "b" in figure 2 pick out the compositional range at $T_3 < T_c$ where the formation of composition-periodical structures would be expected.

3. Noncomplanar Space Periodical Structures

The critical temperature in the alloy diagram denotes the appearance of compositionally inhomogeneous regions with a composition gradient (dx/dr). The free energy (F) of such system may be written:

https://doi.org/10.1557/S1092578300001290 Published online by Cambridge University Press

$$F(x) = \frac{\beta}{2} \cdot \left(\frac{dx}{dr}\right)^2 - \frac{\alpha}{2} \cdot x^2 + \frac{\delta}{4} \cdot x^4 \quad (4)$$

where a, b, d are phenomenological coefficients. The compositional variation of F(x) leads to the Duffing equation [12]:

$$\frac{d^2\Pi}{dy^2} + \Pi - \Pi^3 = 0 \quad (5)$$

The solution of (5) is written through the functions:

$$\Pi(y) = \Pi_0 \cdot sn(\Pi_0 \cdot y / k\sqrt{2}, k); k = \Pi_0 / \sqrt{2 - \Pi_0^2} \quad (6)$$

with a space period $\lambda(\Pi_0) = 4 \cdot K(k) / \sqrt{1 - \frac{\Pi_0^2}{2}}$ which depends on original deviation Π_0, where K(k) is the first order elliptic integral, a ~ T_c - T > 0, y = r/r_c where r_c = d/a is a correlation length, and P = x/x^* where x^* = a/b. The space periodical solution (6) appears only in the range captured by the spinodal. This is schematically demonstrated by curve 3 in figure 1. The conditions of free energy minimization and the existence of temperature gradients in grown samples lead to the fact that the compositional gradient here is normal to the temperature gradient. In other words, layer growth at these parameters is inhomogeneous across the substrate. The space coordinate axis (r) in figure 1 shows the direction parallel to the substrate. An example of another non-complanar structure is the spatial relaxation structure shown in curve 4 of figure 1.

4. Temperature-Composition Dependencies of the Band Gap in Semiconductor Nitrides

The temperature-composition dependencies of the band gaps for each crystal type (AlGaN, InGaN, InAlN) were calculated from (2) taking into account the experimental E_g values of the pure semiconductors [13] [14]. It has been demonstrated that there are three alternative runs of the E_g(x) curve at various growth temperatures. The first is appropriate to InGaN where T_c is slightly lower than the growth temperatures of the mixed crystals [1] [2] [15]. Common temperatures and growth techniques for the nitrides are listed in table 2. Figure 3 shows the result of E_g(x) calculations when the growth temperatures are 700 K, 900 K and 1100 K. The last value is close to the substrate temperature for the MOCVD growth of InGaN crystals. The calculated E_g(x) curve at this temperature is in good agreement with the experimental data at any reasonable bowing parameter (b). It should be noted here that although the bowing factor may be derived from first principles through the effective mass of the electrons in the solution [15], it is doubtful that b can be calculated in this manner. That is why the bowing factor is usually considered as a fitting constant. To determine this parameter we fitted b to experimental data of the alloy band gap variation, but only at small compositions x « 0.5 where b is nearly constant (see table 1).

The other curves in figure 3 show that decreasing the growth temperature leads to anomalous E_g(x). The alloys of InGaN with x ~ 0.5 grown at $T_0 \approx$ 700 K should have near zero band gap. As described above, S_{xx}(x) has discontinuities and a solution with mole fraction x ranging between "a'' and "b'' in figure 2 tends to decompose if the growth temperature is below T_c. Figure 4 demonstrates E_g(x) at $T_0 < T_c$ for AlInN, where this condition is practical, because the critical temperature for this solution (T_c =2116 K) is much higher than the experimental growth temperatures [3]. In this case E_g(x) is a single-valued function only at small concentrations of either component outside the interval between "a'' and "b'' in figure 4. The strange compositional dependence of E_g with very large bowing is observed in the alloy experimentally [3]. Probably such behavior of E_g(x) in AlN-InN at a mole fraction between "a'' and "b'' is caused by the absence of stable (and metastable) states in InAlN alloys at low growth temperature.

https://doi.org/10.1557/S1092578300001290 Published online by Cambridge University Press

The band gap variations throughout the entire compositional range for GaAlN at 77 K (upper curve) and 300 K (lower curve) are shown in figure 5. Here the calculated dependences of $E_g(x)$ have no peculiarities because T_c is well below the growth temperatures for AlGaN [4] [5] [7] [16]. In this case weaker effects begin to dominate. Elastic deformation of the crystal at its cooling from the growth temperature should be taken properly into account for the correction of E_g. Probably the high dispersion of experimental points in papers devoted to AlGaN [4] is explained by non-controlled thermal strain of the crystal layers.

5. Conclusion

The approach to semiconductor solid solutions which takes into consideration their thermodynamic instability states within the framework of the virtual crystal approximation allows the behavior of the alloy bandgap E_g at any composition and temperature to be analyzed. In particular, we were able to estimate the range of convenient growth temperatures and mark the mole fraction range where $E_g(x)$ has an anomaly. Moreover, this approach predicts possible periodic structures in the alloys.

Acknowledgments

The authors would like to acknowledge the financial support of the Russian Academy of Sciences (Grant Nos. 95-02-04148-a and 96-03-32396)

References

[1] S. Nakamura, *Microelectr. J.* ***25***, 651-659 (1994).

[2] S. Nakamura, M. Senoh, N. Iwasa, S. Nagahama, *Jpn. J. Appl. Phys.* ***34***, L797-L799 (1995).

[3] K. Kubota, Y. Kobayashi, K. Fujimoto , *J. Appl. Phys.* ***66***, 2984-2988 (1989).

[4] Y. Koide, H. Itoh, M. R. H. Khan, K. Hiramatu, N. Sawaki, I. Akasaki ,*J. Appl. Phys.* ***61***, 4540-4543 (1987).

[5] I. Akasaki, K. Hiramatsu, H. Amano, *Memories of the Faculty of Engineering, Nagoya University* ***43***, 147-178 (1991).

[6] K. Osamura, K. Nakajima, Y. Murakami, P. H. Shingu, A. Ohtsuki, *Sol. St. Comm.* ***11***, 617 (1972).

[7] A.S. Zubrilov, D.V. Tsvetkov, V.I. Nikolaev, I.P. Nikitina, unpublished (1996).

[8] M. D. Lyutaya, T. S. Bartnitskaya, *Inorg. Mat.* ***9***, 1052 (1973).

[9] R.H. Parmenter, *Phys. Rev.* ***97***, 587-598 (1955).

[10] L.D. Landau, E.M. Lifshitz, *Statistical Physics* (Nauka (in russian), Moscow, 1976) .

[11] G.B. Stringfellow, *J. Phys. Chem. Sol.* ***33***, 665-677 (1972).

[12] N. Moiseev, *Asymptotic methods of nonlinear mechanics* (Nauka (in russian), Moscow, 1969) .

[13] S. Strite, H. Morkoç, *J. Vac. Sci. Technol. B* ***10***, 1237-1266 (1992).

[14] Q. Guo, A. Yoshida, *Jpn. J. Appl. Phys.* ***33***, 2453-2456 (1994).

[15] T. Nagatomo, T. Kuboyama, H. Minamino, O. Omoto, *Jpn. J. Appl. Phys.* ***28***, L1334 (1989).

[16] H.G. Lee, M. Gershenzon, B.L. Goldenberg, *J. Electron. Mater.* ***20***, 621-625 (1991).

[17] S. Nakamura, M. Senoh, N. Iwasa, S. Nagahama, T. Yamada, T. Mukai, *Jpn. J. Appl. Phys.* ***34***, L1332-L1335

(1995).

[18] K. Osamura, S. Naka, Y. Murakami, *J. Appl. Phys.* ***46***, 3432 (1975).

[19] S. Nakamura, T. Mukai, *Jpn. J. Appl. Phys.* ***31***, L1457-L1459 (1992).

[20] H. Sakai, T. Koide, H. Suzuki, M. Yamaguchi, S. Yamasaki, M. Koike, H. Amano, I. Akasaki, *Jpn. J. Appl. Phys.* ***34***, L1429-L1431 (1995).

Table 1

Figure 1. Bowing parameters and critical temperatures for nitride semiconductors.

Alloys	GaInN	AlInN	AlGaN
Tc, K	680	2116	320
b	0.6	1.2	0.7

Table 2

Growth techniques, technological temperatures and experimental procedure for nitride alloy research. EPMA is electron probe microanalysis; PL, EL are photo- and electroluminecsence, respectively.

https://doi.org/10.1557/S1092578300001290 Published online by Cambridge University Press

Growth technique, [Ref.]	samples	growth temperatures T_0	composition determination	E_g investigation technique	notes/problems
MOVPE [15]	$In_xGa_{1-x}N$ $0 \leq x \leq 0.42$	450-950 °C	XRD, fluorescent spectroscopy	absorption edge	$E_g(x=0.42) \cong E_{InN}$ at $T_0 = 500$ °C
Electron Beam plasma technique [6] [18]	$In_xGa_{1-x}N$ $0 \leq x \leq 1$ polycrystalline film	Long time annealing at 600 - 800 °C	XRD	absorption edge	alloy decomposition at $T_0 \approx 200$ - 500 °C
MOCVD [19]	$In_xGa_{1-x}N$ $0.14 \leq x \leq 0.24$	780 °C 830 °C	XRD,	PL	
RF-MBE [20]	$In_xGa_{1-x}N$ $0 < x < 0.2$	930 K	–	PL	
MOCVD [1]	$In_xGa_{1-x}N$ $0.07 < x < 0.33$	720-850 °C	XRD	PL	
MOCVD [2] [17]	$In_xGa_{1-x}N$ $0.2 < x < 0.7$ SQW	–	–	EL, band edge emission	shift edge emission in SQW
RF magnetron sputtering [3]	$In_xAl_{1-x}N$ $0 \leq x \leq 0.4$, x = 1	$T_0 < 500$°C	XRD,	absorption edge	
MOVPE [4] [5]	$Al_xGa_{1-x}N$ $0 \leq x \leq 0.4$	1000 °C	XRD, EPMA	absorption edge	
MOVPE [16]	$Al_xGa_{1-x}N$ $0 \leq x \leq 0.7$	–	XRD, EPMA	absorption edge, PL	

https://doi.org/10.1557/S1092578300001290 Published online by Cambridge University Press

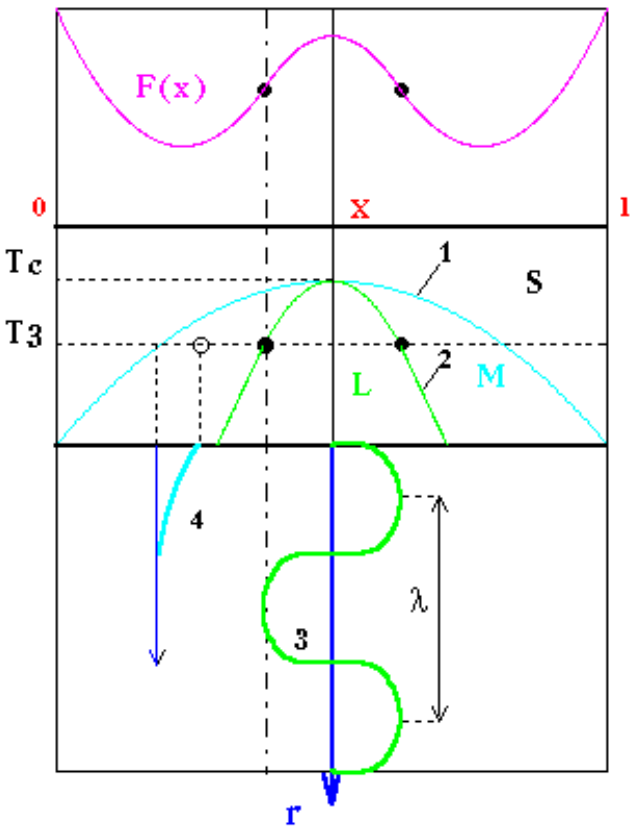

Figure 1. Temperature-composition diagrams for the regular solution and examples of the space structures. F(x) is the compositional variation of the free energy at $T_3 < T_c$. The curves 1 and 2 are the binodal and the spinodal respectively. Curve 3 schematically shows the space periodical structure at T_3 in the labile (L) states of the solution (the area of lability is under the spinodal). Curve 4 demonstrates the space relaxation structure in the region of metastable (M) states of the solutions (between curves 1 and 2). S marks the area, where the solution is stable.

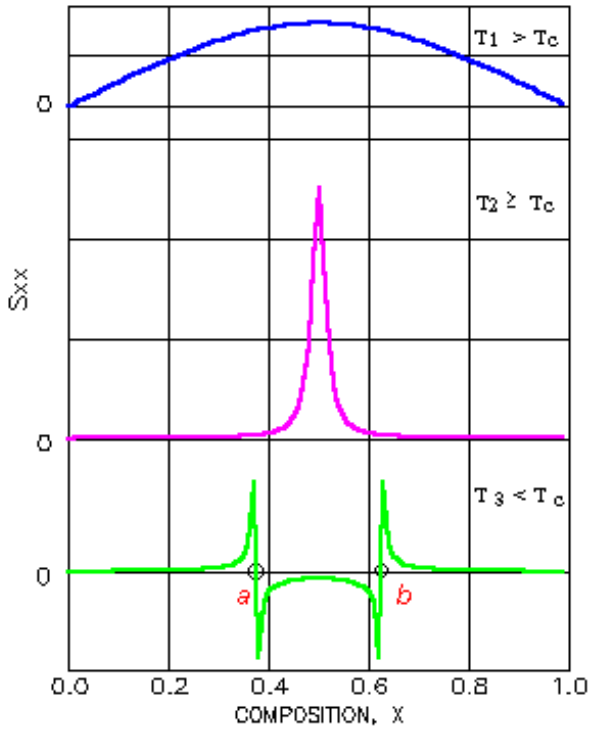

Figure 2. Compositional dependence of S_{xx} at various temperature.

https://doi.org/10.1557/S1092578300001290 Published online by Cambridge University Press

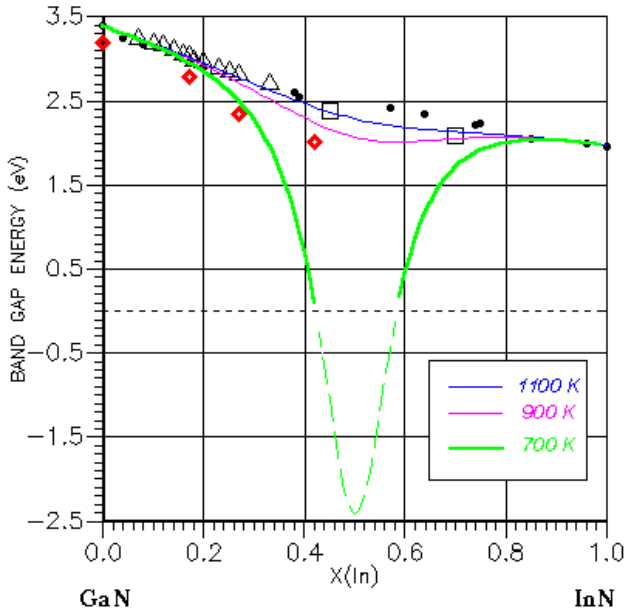

Figure 3. Variation of the direct energy band gap E_g with x for $In_xGa_{1-x}N$ at room temperature. The curves show $E_g(x)$ calculated from (2) at various "growth" temperatures. The dashed line marks the range where term E_g loses its ordinary meaning. The symbols are experimental data: (•) represents E_g of the polycrystalline alloys grown by electron beam plasma technique from mixtures of Ga and In (Osamura et al. [6]); (Δ) and (open squares) represent E_g of high quality single crystal layers grown at the temperature from the range 1050-1100 K and LEDs (Nakamura et al. [1] [2] [17]); (red diamonds) represent E_g of the single crystal alloys grown by MOVPE at about 770 K (Nagatomo et al. [15]).

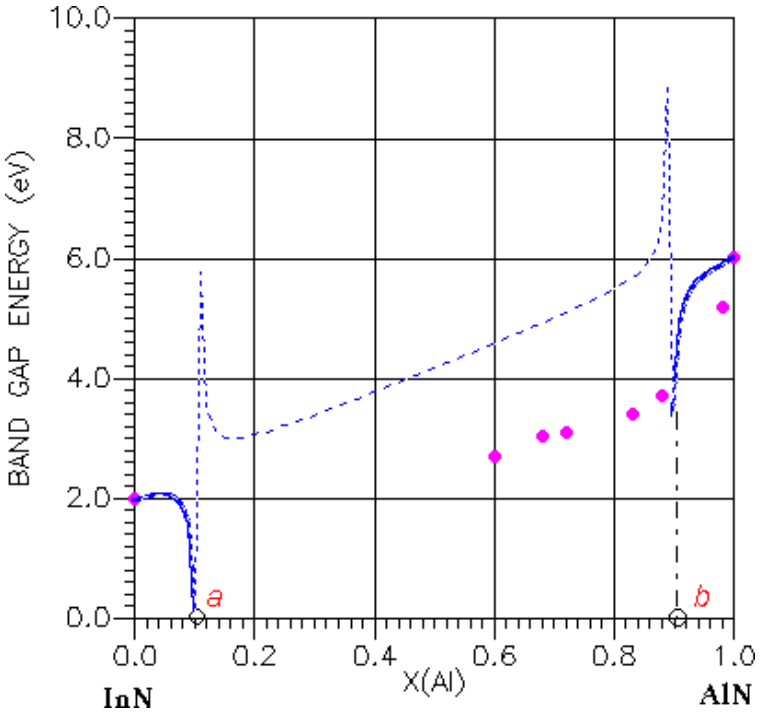

Figure 4. Variation of room temperature $E_g(x)$ for $In_xAl_{1-x}N$ alloys grown at temperature T_0 = 800 K. The curve represents the calculated dependence of $E_g(x)$, the dashed line marks the range where the $E_g(x)$ is not uniquely determined. The dots show the data from [3].

https://doi.org/10.1557/S1092578300001290 Published online by Cambridge University Press

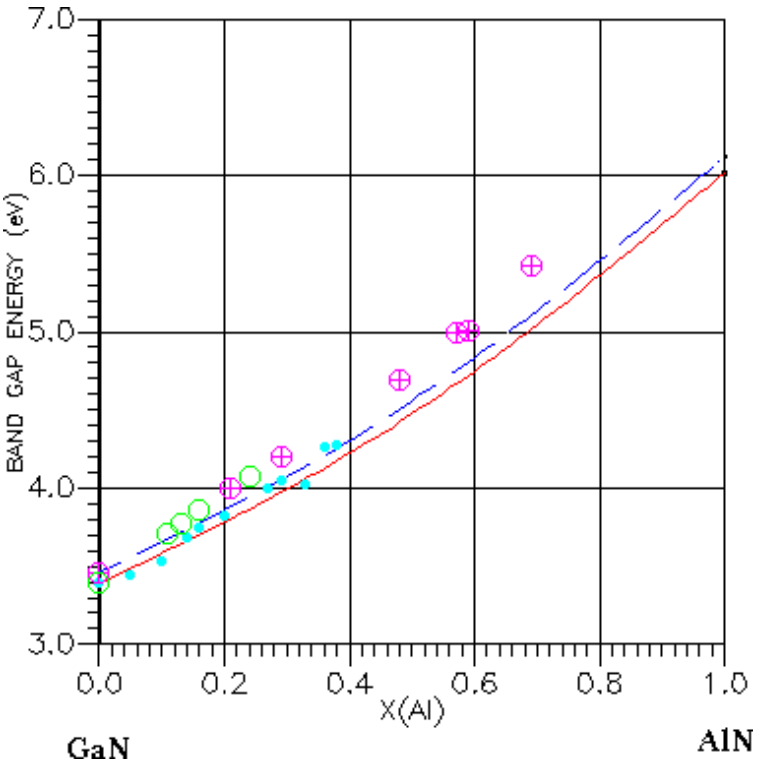

Figure 5. The compositional dependence of the band gap in $Al_xGa_{1-x}N$ alloys at 77 K and 300 K. The curves are calculated from (2) for alloys grown at 1300 K. The solid curve is $E_g(x)$ at room temperature and the dashed curve is $E_g(x)$ at 77 K. The circles represent experimental data; the filled circles from [4], open from [7], both at the room temperature; and crossed out circles are experimental values of E_g at 77 K [16].

M R S Internet Journal of Nitride Semiconductor Research

https://doi.org/10.1557/S1092578300001290 Published online by Cambridge University Press